Selectivity-permeability optimization of functionalised CNT- polymer membranes for water treatment: A modelling study

Federica Bisignano,[1] Davide Mattia,[2] Giorgio De Luca*[1]

[1]Research Institute on Membrane Technology (ITM-CNR), University of Calabria, Via P. Bucci, I-87036 Arcavacata di Rende (CS), Italy
[2]Department of Chemical Engineering, University of Bath, Bath, BA27AY, UK

Abstract

Polymer membranes incorporating carbon nanotubes (CNT) belong to two broad categories: Vertically aligned (VA-CNT) membranes, where the polymer acts solely as a matrix embedding an aligned forest of nanotubes, and thin film composite (CNT-TFC) membranes which incorporate randomly aligned nanotubes in their selective layer. The former can achieve orders-of-magnitude higher permeability than many commercial membranes but cannot be scaled up industrially. The latter are based on commercial technology but provide only modest flux increases. Furthermore, filtration in VA-CNT is based on steric hindrance determined by the tubes' diameter, whereas in CNT-TFCs, the tubes are embedded in the polymer with selectivity given by the polymer alone.

In this work, a novel computational method to optimize the selectivity-permeability of an ideal CNT membrane encompassing the advantages of VA-CNTs and CNT-TFCs is presented. In analogy to the former, the tubes are all aligned with the membrane selectivity provided by their diameter; to the latter, the polymer matrix also contributed to the total membrane permeability. As nanotubes with larger internal diameter would provide higher flow, *ab-initio* modeling was used to improve their selectivity by functionalizing the tips of large multiwall nanotubes with PIM-1 monomers, achieving simultaneously an increase in selectivity towards small molecules (e.g. rac-Fluoxetine, glucose, ethanol and water) and an increase in permeability (due to the large diameter). Results show up to 3 orders of magnitude increase in water permeability compared to a CNT-TFC membrane in the literature with randomly oriented tubes of comparable size and an increase in rejection of a factor of 2.5 and 2, for rac-fluoxetine and glucose, respectively, compared to water. The proposed methodology is of general use and requires no fitting parameters, only the chemical structure of the solutes to test and the tubes' geometry.

**Corresponding Author: Giorgio De Luca, Phone: +39 (0984) 492080. Fax: +39 (0984) 402103. E-mail: g.deluca@itm.cnr.it. Homepage: www.itm.cnr.it*

Keywords: carbon nanotubes; thin film composite membrane; ab-initio modeling

Graphical Abstract

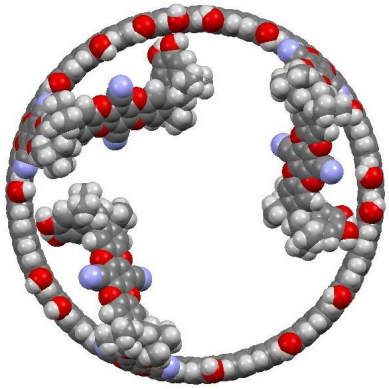

Functionalization of CNTs inlet to maximize molecule rejection and water permeability

1. Introduction

In membrane-based filtration processes, permeability and selectivity are considered key performance parameters and, in general, the increase of the former comes at the expense of the latter. Mixed-matrix membranes, where a second phase is added to a polymer matrix to enhance either characteristic, emerged as the most promising technology to further reduce the energy cost and improve performance of membrane-based filtration processes. Among the many materials considered as potential additives, carbon nanotubes (CNT) have attracted the most interest due to promise of ultra-low transport resistance. The first published molecular dynamics simulation of water flow inside a single-wall carbon nanotube (SWNT) with a diameter of 1 nm or less showed very high flow rates [1], initially described in terms of ballistic transport [2] and attributed to the hydrophobicity of the nanotube's wall in respect to water [3]. As further modelling and experimental results have confirmed initial observations, interest shifted to measuring the performance of carbon nanotube membranes rather than flow in individual nanotubes [4]. A recent analysis by the authors shows that the orders-of-magnitude water high flow rates observed in single tubes do not automatically translate in orders-of-magnitude higher membrane permeability but rather smaller, yet still significant, increases [5]. This difference can be attributed primarily to the geometrical and structural characteristics of the CNT membranes, which, in turn, are a result of the fabrication methods available.

The first carbon nanotube membranes produced were all so-called vertically aligned carbon nanotube (VA-CNT) membranes: These were manufactured using an aligned array of CNTs produced via catalytic chemical vapour deposition on silicon/silicon oxide substrates. The array was then infiltrated with polymer [6-8] (or embedded within an inorganic matrix [9]) to provide mechanical stability and prevent leaks, detached from the substrate and the tube ends opened. These membranes usually have a filtration area of 1 cm^2 or less [10]. These membranes also tend to have low tube density (equivalent to porosity), which decreases performance. A molecular dynamics study of highly-packed and aligned SWNTs in a periodic cell has shown theoretical permeability increases of over 3 orders of magnitude compared to a commercial RO membrane with salt rejection close to 100% [11]. When the tube density was reduced to what can be currently achieved experimentally, a much smaller permeability was observed. An alternative technique deposited turbostratic carbon in the pores of alumina nanoporous templates, creating what have been called nanopipe structures [12]. Unfortunately, none of these

techniques can actually be scaled economically to a level where they can supply the wastewater membrane market [4].

A more practical route has emerged, incorporating randomly oriented multi-wall carbon nanotubes (MWNTs) dispersions in the active layer of thin film composite (TFC) polymer membranes or polymeric matrices [13]. A large number of nanotube-polymer membranes have now been fabricated with varying performance: A 4-fold increase in permeability with no loss in salt rejection was observed in polyamide TFC membranes with 20 wt% MWNTs loading [14] compared to the virgin one. Another MWNT/PA TFC membrane saw a 6% decrease in flux compared to the reference without tubes but an increase in rejection for salt and humic acid (MWNT loading ~1 wt%) [15]. A 4-fold increase in flux was also observed for a 10wt% MWNT/chitosan membrane [16], whereas a 2-fold increase was observed for randomly aligned MWNT/polyester TFCs [17]. A negligible increase in permeability, on the other hand, was observed for a MWNT/polysulfone (MWNT loading varying from 1 to 4 wt%) [18].

Although most studies on CNT membranes have, so far, focused on maximizing permeability, some work has been done on CNT membrane selectivity, particularly salt rejection for RO applications. As steric-only rejection requires extremely small tubes with a negative effect on permeability – for example, to reject a 200 Da molecule a SWNT with diameter of 1 nm or less would be required – functionalization of the nanotube inlet has emerged as a more practical alternative [19]. Charge-based selectivity was significantly increased when the tips of a MWNT-polymer membrane were functionalized with alkanes and amines, attached to the tubes via carboxylic defects created on the tubes' tips [20]. MD studies on CNT functionalization for seawater desalination have shown that the addition of charges on the tip of a 1.1 nm SWNT can reduce the passage of ions but at the expense of water permeability [17]. Another MD study showed the effect on salt rejection and permeability of a SWNT membrane of several different functional groups grafted onto the tube tips [11]. Results showed that functionalization reduced flux in all cases, with the largest reductions occurring for the bulkiest functional groups and those with the strongest charge density. For the same reasons, ion rejection increased in the functionalized tubes compared to the pristine ones.

All these large variations can be attributed to two main factors: first, carbon nanotubes are actually a family of materials, whose properties can vary significantly due to the synthesis process used, from geometrical characteristics (diameter and length) to the surface structure (from turbostratic to highly

organized graphitic) to the surface chemistry (from hydrophobic to hydrophilic) [3, 21]. MD studies have confirmed that the presence of defects [22], the structure of the tubes [23] and their length [24] all affect water flow through the tubes. A recent theoretical model by the authors has shown that these apparent discrepancies can be resolved by normalizing modelling and experimental flow rates for the tubes' geometrical characteristics and solid-liquid molecular interactions [23, 25, 26]. Second, as the tubes are randomly aligned (in TFCs), there is little to no control on the degree of orientation of the tubes, leading to varying performance [27].

In this publication, a novel computational methodology, free of adjustable and empirical parameters, to maximize both water permeability and selectivity for functionalized carbon nanotube-polymer membranes, is presented. The aim is to provide a computational strategy to design bespoke CNT-polymer membranes for specific filtration applications, maximizing both permeability and selectivity. As a demonstration of the proposed method, the functionalization of the tips of large multi-wall nanotubes with organic monomers to reject small solutes, difficult to separate from water, is presented.

2. Materials and Modelling Approach

An ideal MWNT-polymer membrane is considered in this modeling study where all the nanotubes are perpendicularly aligned to the membrane's surface in a polymeric matrix with no voids present between the polymeric matrix and the tubes (as in a VA-CNT membrane) but with the polymer matrix also contributing to permeability (as in a CNT-TFC). Two cases from the recent literature are used as reference, one a polyester TFC asymmetric membrane [17] and the second a chitosan porous membrane [16] both containing randomly aligned MWNTs embedded in the polymer with no direct access to the feed. For the first membrane, the thickness of the selective layer is approximately 500 nm with a total membrane area of 27 cm^2. The measured pure water flux was ~10.8 $Lm^{-2}h^{-1}$ (LMH) at 0.6 MPa and room temperature for the membrane containing no nanotubes. The flux increased to ~21.8 LMH under the same conditions, when 0.5 mg/ml of MWNTs (external diameter, D_{CNT} < 8 nm; internal diameter, d_{CNT} = 2-5 nm; L= 10-30 μm) was added to the aqueous phases during the phase inversion process. The chitosan membrane presents a mean thickness of the wet membrane of about 130-140 μm and a membrane area of 11.33 cm^2. The pure water flux was ~28 LMH at 0.1 MPa without MWNTs. The flux increased to ~120 LMH at 0.1 MPa with 10wt% of MWNTs (D_{CNT} = 10-30 nm; L= 5-15 μm).

2.1 Permeability optimization

When considering MWNTs, the thickness of the tubes has to be considered in the calculation of the effective CNT permeable area:

$$A_{CNT,eff} = \sum_{i=1}^{n} \pi \frac{d_{CNT,i}^2}{4} \equiv n\pi \frac{d_{CNT}^2}{4} \quad (1)$$

where *n* the total number of tubes vertically trapped in the membrane while d_{CNT} is internal diameter of the MWNT. On the other hand, the membrane surface fraction occupied by the MWNTs is:

$$f = \frac{A_{CNT}}{A_{mem}} = \frac{1}{A_{mem}} \sum_{i=1}^{n} \pi \frac{D_{CNT,i}^2}{4} \equiv n\pi \frac{D_{CNT}^2}{4A_{mem}} \quad (2)$$

where A_{mem} is the total membrane area, A_{CNT} is the total area occupied by the MWNTs, and D_{CNT} is the 'external diameter' of the MWNTs. The above relationships assume no size distribution for the nanotubes, a constant cross-section throughout their length and tortuosity, τ=1. With these assumptions, *f* is equivalent to a standard surface porosity and its maximum value is 0.74, following standard geometrical rules [11]. For the multi walled CNTs, $A_{CNT,eff} < A_{CNT}$, whereas for a SWNT it is assumed that $D_{CNT} \equiv d_{CNT}$, with this value being the distance between the CNT carbon nuclei. Only MWNTs have been considered in this work due to their lower cost compared to SWNT with equal characteristics and internal diameter. Two values, 35 and 15 nm, have been chosen for D_{CNT}, representative of the wide range of commercially available MWNTs. For the innermost tube diameter, d_{CNT} values of 1.66, 2.22, 2.77, 3.33, 3.88, 4.44 and 4.99 nm have been selected following well-known nanotube dimensioning rules [28].

How liquid flow in CNTs can be described is a matter of current debate, as pointed out in the introduction. In this paper the uncertainty on which model to adopt is side-stepped by relying on numerical data extracted from a well-known molecular dynamics paper [29] as:

$$Q_{CNT} = nq_{CNT} = n\alpha \frac{\Delta P}{L} \quad (3)$$

where q_{CNT} is the flow rate in a single carbon nanotube and $\Delta P/L$ is the applied pressure gradient. α is a proportionality constant obtained from the numerical analysis of the aforementioned MD simulation that incorporates all effects of nanotube radius (here this radius is $d_{CNT}/2$), structure, fluid viscosity and

solid-liquid interaction on flow, without making them explicit. It is important highlight that this method is of general use and not limited to the conditions set in [29], and it could be applied to flow data extracted from other publications for different liquids and/or tubes. The total flow rate of the MWNT-composite membrane, $Q_{mem,f}$, is defined as the sum of the water flow through the nanotubes and the water flow through the remaining free area of the membrane, i.e. the free membrane fraction area not occupied by the CNTs, $(1-f)$:

$$\mathrm{Q_{mem,f}} \equiv \mathrm{Q_{CNT}} + \mathrm{Q_{mem,0}}(1-\mathrm{f}) \tag{4}$$

where $\mathrm{Q_{mem,0}}$ is the water flow of the pristine membrane which depends only on the operating conditions and membrane type. Dividing by $Q_{mem,0}$ yields:

$$\frac{\mathrm{Q_{mem,f}}}{\mathrm{Q_{mem,0}}} = \frac{\mathrm{Q_{CNT}}}{\mathrm{Q_{mem,0}}} + (1-\mathrm{f}) \tag{5}$$

where the ratio $\mathrm{Q_{mem,f}}/\mathrm{Q_{mem,0}}$ is the change in overall flow rate given by the presence of CNTs occupying a fraction f of the membrane surface. To compare modelling results with experimental data coming from different CNT membranes, $\mathrm{Q_{mem,f}}/\mathrm{Q_{mem,0}}$ can also be reported in terms of permeability, $K = QL/\Delta PA$, i.e. by dividing and multiplying Eq. (5) by $L/\Delta PA_{mem}$:

$$\frac{\mathrm{K_{mem,f}}}{\mathrm{K_{mem,0}}} = \frac{\mathrm{K_{CNT}}}{\mathrm{K_{mem,0}}} + (1-\mathrm{f}) \tag{6}$$

where A_{mem} is the experimental total area of the membrane and L/ΔP is defined by the corresponding experimental data.

2.2 Selectivity optimization

In this work, molecular sieving by carbon nanotubes is based solely on steric hindrance [30]. The selectivity of the MWNTs was evaluated through a morphological and topological analysis of the target compounds and the nanotube grafted with functional groups (FGs) on its tip. As reported in several

steric-hindrance pore models, the sieving coefficient is generally evaluated as function of the ratio between solute and membrane pore size, obtained from experimental data [30, 31]. When the solute size is larger than the pore size, it cannot permeate through the membrane resulting in 100 % rejection. However, when the pore inlet is decorated with chemical groups, it can be challenging to obtain an unambiguous pore size value, without resorting to simplifying assumptions and fitting procedures with the risk of losing the physical sense of the phenomenon. To address these limitations, in this work, an algorithm to evaluate the rejection of CNTs without introducing adjustable parameters is proposed. The algorithm is based on the computation of the fraction of the functionalized inlet area through which solutes permeate with no steric hindrance. Therefore, the rejection (R) of target compounds, here, is assumed to be proportional to $1-\Sigma$, (i.e. $\mathrm{R} \propto 1-\Sigma$) where:

$$\Sigma = \frac{A_{mol,perm}}{A_{CNT,free}} \tag{7}$$

where $A_{CNT,free}$ is the maximum free area of the functionalized nanotube inlet and $A_{mol,perm}$ is the effective molecular permeation area (Fig. 1a). The former is calculated considering the ensemble of CNT free inlet points. These are all the points on the inlet excluding the projections of the rigid spheres that constitute the functional groups atoms. Without FGs on the border of the nanotube, $A_{CNT,free}$ is reduced to the inlet area excluding the thickness of the carbon, hydrogen and hydroxyl atoms. When the FGs are present, $A_{CNT,free}$ is evaluated by the sum of the areas of the disjoint circular and annular grid sectors free of the projected FG spheres [32]. This means that the term $A_{CNT,free}$ represents the actual functionalized pore shape (Fig.1a) rather than an approximate one obtained via fitting, as in previous models.

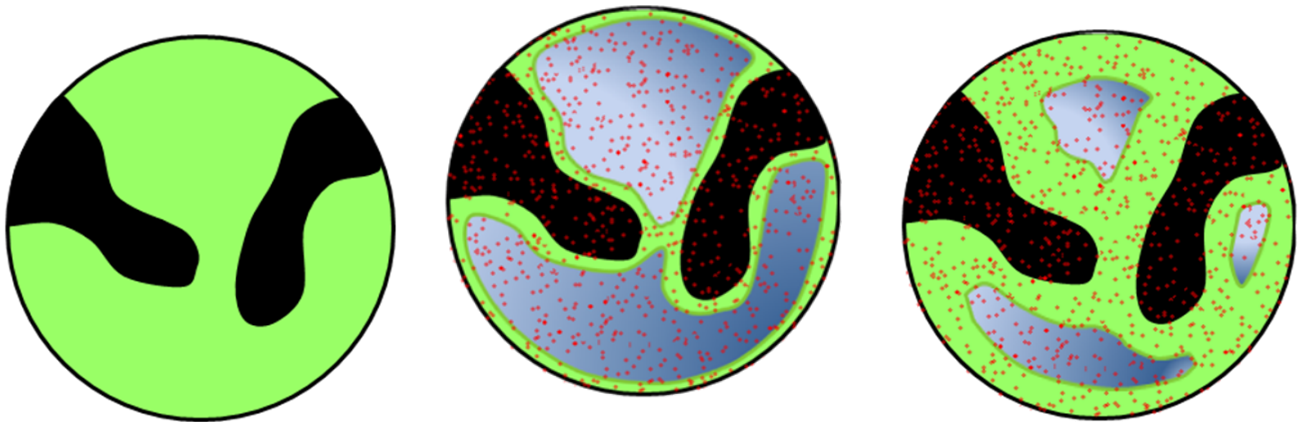

(a) (b) (c)

Figure 1: Top view of a functionalized CNT: (a) in black is the area covered by two FGs, in green is $A_{CNT,free}$ and in blue is $A_{mol,perm}$ for a sample with (b) small and (c) large MCS.

The points characterizing the $A_{mol,perm}$ area are a subset of $A_{CNT,free}$ points ($A_{mol,perm} \leq A_{CNT,free}$) and they depend on the shape and sizes of the solute to be rejected, which here were evaluated from the optimized geometries of solutes at the quantum level. Specifically, the points of the $A_{mol,perm}$ are calculated considering the inlet *free* points through which the target molecule can permeate with no steric hindrance both due to the CNT edge and the anchored functional groups. This is achieved by a statistical procedure generally used to estimate the area of complex (irregular) geometric shapes. In particular, starting from a known number of points randomly located in the CNT pore area, this procedure checks if a probe is inside or outside the boundary of the irregular shape. The details of the algorithm used to calculate $A_{mol,perm}$ and $A_{CNT,free}$ are reported in [32].

Since in $A_{mol,perm}$ the main role is played by the dimensions of the target solutes, an accurate morphological analysis of solute optimized geometries was carried out, in particular evaluating the molecular minimum-cross section (MCS) of each solute. Each optimized compound was modeled as a van der Waals solid such that each atom is represented by a hard sphere with a specific radius. The MCS was then defined as the minimum rectangle enclosing the orthogonal projections of all atoms of the target molecule on a plane perpendicular to the principal molecular axis [32, 33]. The minimum rectangle allows taking into account all the projection of the atoms of the solute while minimizing the empty space, unlike a circular domain which overestimates the minimal cross-section of the molecules

[32]. This approach ensures that the shape of the molecules is not lost when considering the MCS since it takes in account all the atom projections of the solutes.

The steric hindrance of a molecule in the vicinity of a pore inlet is minimal if it is placed according to its MCS, implying that if the molecule is rejected in this orientation, it will also be rejected in any other spatial orientation with respect to the nanotube's entrance [34]. For example, a top view of a functionalized CNT is shown in Figure 1, in which the $A_{CNT,free}$ and $A_{mol,perm}$ areas for two target molecules with different MCS are shown; $A_{mol,perm}$ decreases with increasing solute size, whereas $A_{CNT,free}$ decreases with steric hindrance of the grafted FG. It is worth pointing out that $A_{mol,perm}$ and $A_{CNT,free}$ as well as the evaluation of the MCS do not depend on any adjustable parameter. On the contrary, they are only based on a topological and morphological analysis of the functionalized CNT inlet and solute geometries, optimized via an accurate *ab-initio* quantum mechanics approach.
It is worth noting that other factors can control the sieving, such as the flexibility of the FG spiro-centre and hydrogen bonding with the ether linkages. The flexibility of the spiro group and, in general, of the whole FG, is roughly taken into account by means of the energy difference between the initial geometry of FG and those obtained after the quantum optimizations or from the second derivative of the optimized FG total energy. In fact, the FGs equilibrium geometries are minima on the potential energy surface, thus the energy to distort these equilibrium geometries is related to the flexibility of these groups. Hydrogen bonds were not considered in this work and represent scope for future investigation.

2.3 Molecular models and computational details

A common low molecular weight therapeutic compound, rac-Fluoxetine, widely found in wastewater and whose removal is currently considered challenging, was selected as solute sample in this study, in addition to glucose, ethanol and water. Since the MWNTs selectivity is ruled by the size of the innermost carbon tube, only the functionalization of the MWNT inner inlet is considered. In particular, the functionalization of hydroxyl groups randomly arranged along a CNT inlet of 4.44 nm was modeled. The choice of this diameter will be justified in the next section. As functional groups, monomers of polymers of intrinsic microporosity (PIM) [35] were considered for their controlled, rigid structures. The molecular rejection is based mainly on a size exclusion mechanism. A detailed description of the functionalization procedure can be found in the supplementary information section. In Fig. 2 and Table

S1 are summarized all the FGs studied and, hereinafter, identified with the symbol: A or B, according to the initialization steps (reported in supplementary information), the number of PIM-1 monomers (i.e. n=1 or 2, 1A or 2B) and furthermore by the number of single anchored FGs (e.g. 2,1A or 3,2B). Finally, the configurations of the functionalization models, i.e. IN or OUT, were indicated as a superscript on the corresponding symbols. The A and B models differ based on the corresponding hooks used to anchor the FGs, as shown in Fig. S1a,b and Fig S2. Two hooks were used in this modeling study because the hydroxyl anchoring groups, according to their concentration, are randomly distributed along a CNT border. Thus, different arrangements of -OH groups on the tubes' tips can be found, as shown in Fig. S3. For example, if two hydroxyl groups are located on adjacent carbons atoms of the CNT inlet, in this case the A hook would be advised. Instead, with two -OH groups arranged on non-neighboring carbon atoms, the B hook would be recommended.

Figure 2: Top view of the functionalized CNT tips: four A models pointing inside (a, b) and outside (c, d) respectively, two B models pointing simultaneously inside and outside (e, f).

The optimization of the FGs and solutes geometries (Fig. 2) was carried out at quantum mechanics level, in the framework of Density Functional Theory (DFT), by using the NWChem code [36]. Exchange-correlation, X3LYP [37], hybrid functional and large basis sets (6-311++G**) were used for the optimization of the solute geometries. Due to the large size of the proposed FG models, the optimization of their structures was carried out with relatively small basis sets (3-21G*). For the CNT model, whose Cartesian coordinates were frozen during the FG optimization, a minimal basis set was used. Specifically, an initial optimization was carried out considering the A or B hooks as shown in Fig. S4. In fact, it is important to emphasize, as will be pointed out in the next section, that the hook inclination is a key aspect to selecting the best functional chemical group as it determines the steric hindrance of the entire functional group. For this reason, the hook's inclination with respect to the pore plane was investigated in detail as shown in Fig.s S4 and S5. Hence, based on the FG inclination and analyzing the 1-Σ values, a large number of FGs, such as oligo-ethylene glycol and silanes groups [38-40] (not reported here), were screened and discarded as unsuitable. The FGs based on PIM-1 monomers were instead chosen as providing the best combination of chain rigidity and coverage of the tubes' inlets. As noted in section 2.2 the optimization of the FGs provides equilibrium structures; as a

result it is also possible to evaluate the FG stiffness by calculating the energy required to distort the FG from its equilibrium geometry, i.e. evaluating the second derivatives of the total energy. This analysis has shown that the PIM-1 monomers based FGs provide a good chain rigidity (not reported here).

The full geometries optimization of the PIM-1 monomer based FGs was carried out by means of the so-called ONIOM quantum approach [41, 42]. This quantum method enables different levels of DFT theory to be applied to different parts of the system. Precisely, the A and B hooks were taken into account at high-level theory, while the remaining parts of the FGs were treated at lower levels of theory, i.e. Slater /3-21G [43]. For the total energy convergence threshold, the energy gradients and the Cartesian atom displacements used in the geometry optimizations, the default criteria adopted by the NWChem code [36] were used in all the quantum-based calculations. NWChem 6.1 code provides scalable methods to treat scientific computational chemistry issues in efficient ways. Since the distortion of the solute geometry due to the presence of FGs attached to the edge of the CNTs is insignificant given their small size compared to the considered CNT inlet, in the subsequent analysis the optimization of their structures was carried out without considering the effect of the pore entrance.

3. Results and discussion

3.1 Permeability prediction

In Fig. 3 the permeability ratio *versus f* is presented for vertically aligned MWNTs within the selective layer of a TFC membrane.

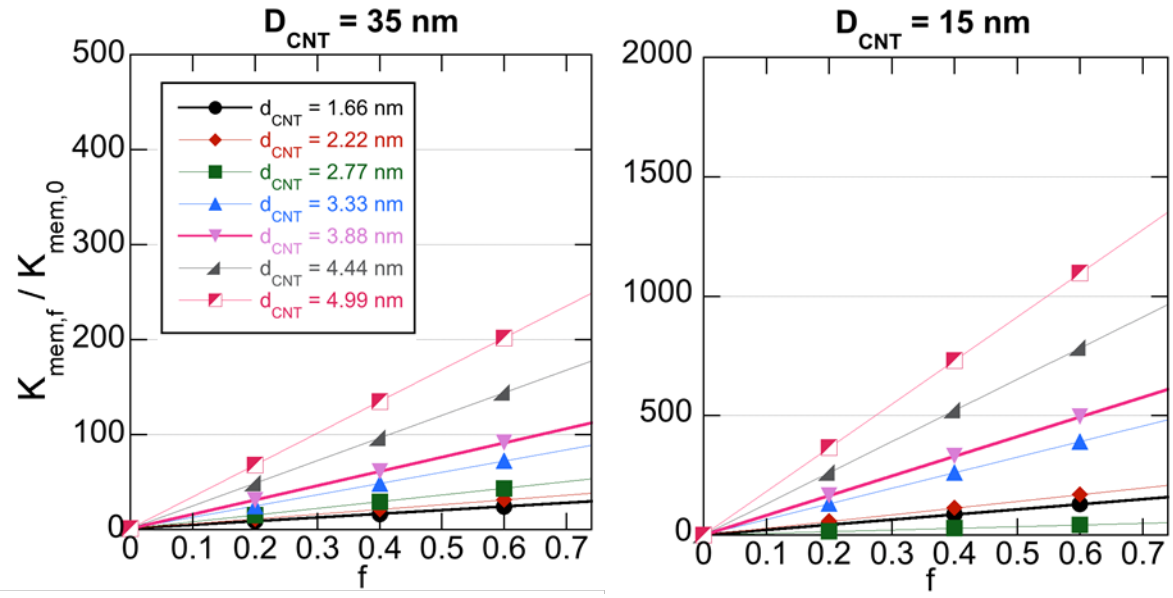

Figure 3. Water permeability increase *versus* surface area fraction occupied by MWNTs, *f*, for a MWNT polyester TFC membrane for two external MWNT diameters (35 and 15 nm) and different inner nanotube diameters; (for $f = 0$ $\frac{K_{mem,f}}{K_{mem,0}} = 1$)

For a fixed external diameter of the MWNTs, according to Eq. 6 the water permeability depends linearly on the fraction of membrane surface area occupied by the tubes, *f*, which is related to the external tube diameter. To evaluate the dependence of the permeability on the internal MWNT diameter, one has also to consider Eq. (1). As a result, the change in the internal tube diameter, for a fixed external tube diameter, leads to a significant variation in overall permeability with an 8-fold increase in passing from 1.66 to 4.99 nm. Even more significant are the increments of permeability obtained by reducing the external diameter of tested MWNTs. In fact, in passing from external tube diameters of 35 to 15 nm, permeability increases 5-6-times for the same internal tube size and constant *f*. These results were achieved assuming no water flow through the interlayers between nanotubes in the MWNT. Through the relatively simple relation in Eq. (6), it is possible to optimize the external MWNT diameter as function of the performance required for a specific CNT membrane.

For $f = 0.4$, $D_{CNT} = 15$ nm, $d_{CNT} = 4.44$ nm, there is about a 500-fold increase compared to the virgin membrane (Fig. 3), with an absolute value of ~ 900 LMH at 1 bar. The best permeability for the TFC with randomly oriented tubes used as reference [17] is ~ 3.6 LMH at 1 bar, compared to a value of ~ 1.8 LMH at 1 bar. The tubes in this work and in [17] have comparable inner diameters, while the former have a larger outer diameter than the latter, which works against the present case. One could argue that the difference might be due to a different volume fraction (or number) of tubes in the two membranes. Although in [17] the volume fraction of MWNTs in the membrane is not reported, a per mass comparison can be attempted: Assuming a CNT density of 1.4 g/cm^3 [28], the mass of aligned MWNTs present in the present model membrane is estimated, from Eq. (2) and total membrane area, to be ~2.5 mg. In [17], the authors used aqueous solutions containing from 0.2 to 2.0 mg_{MWNT}/ml_{water} in the preparation of the MWNT-TFC membrane. Therefore, and on a qualitative basis only, it appears reasonable to assume that the number of MWNTs in the two membranes is comparable, making the permeability comparison meaningful.

Similar simulations carried out for the asymmetric chitosan porous membrane showed remarkably different results: In fact, the inclusion of vertically aligned MWNTs results in a decrease of the total

water permeability (Fig. 4). This trend can be explained by considering that the virgin chitosan membrane itself is extremely water permeable and the addition of MWNTs only results in loss of its highly permeable membrane surface since the water cannot flow through the MWNTs interlayers.

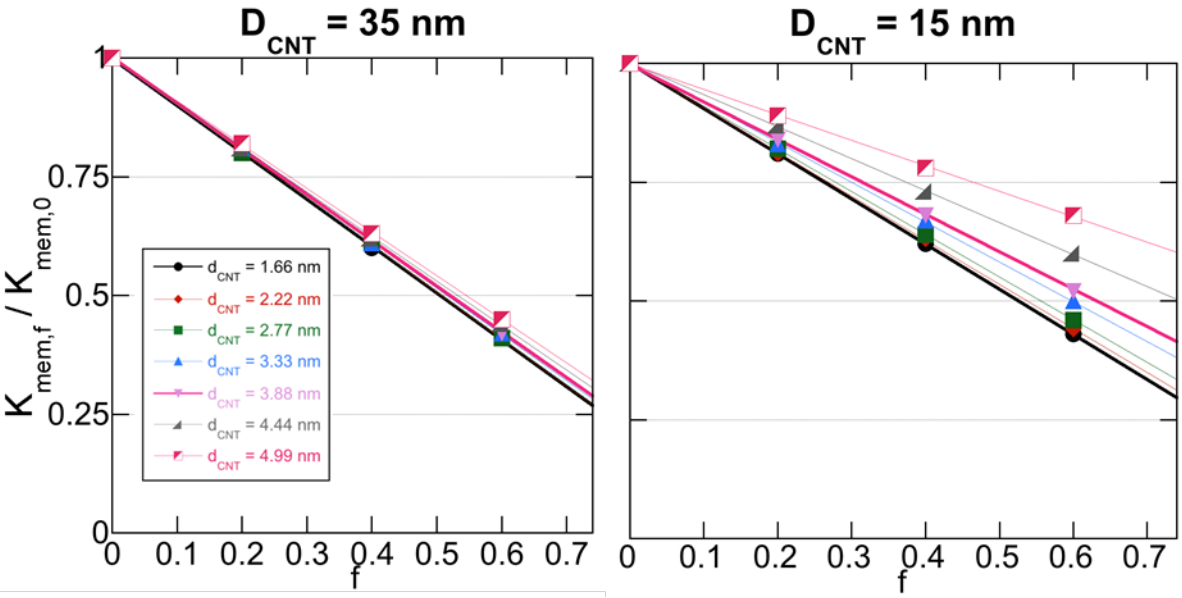

Figure 4. Water permeability increase versus surface area fraction occupied by MWNTs f, for a MWNT chitosan membrane for two external MWNT diameters (35 and 15 nm) and different inner nanotube diameters.

Thus, the water flow enhancement that would be provided by the innermost nanotube of the MWNT is not enough to compensate the loss in flow caused by the reduction of the permeable membrane surface. This result highlights the importance of considering the nanotubes' wall thickness when evaluating the permeability of a membrane containing nanotubes.

An increase in water permeability could be achieved if thin MWNTs were used, as shown in Fig. 5, where double-wall carbon nanotube of different dimensions [44] are considered, resulting, however, only in a modest increase in the overall permeability.

Moreover, it is worth noting that contrary to the TFC membrane, in this case the increase in overall permeability is not directly correlated to the internal nanotube diameter, because the same water permeability enhancement is achieved for internal diameters equal to 1.66, 3.33 and 3.88 nm, respectively.

As single- and double-wall nanotubes are significantly more expensive than MWNTs, it is reasonable to argue that the additional cost and complexity of incorporating S/DWNTs in membranes to increase their permeability is justified for low permeability membranes, such as the polyester TFC (Fig. 3) but not for those that already have a relatively high one (Fig. 5).

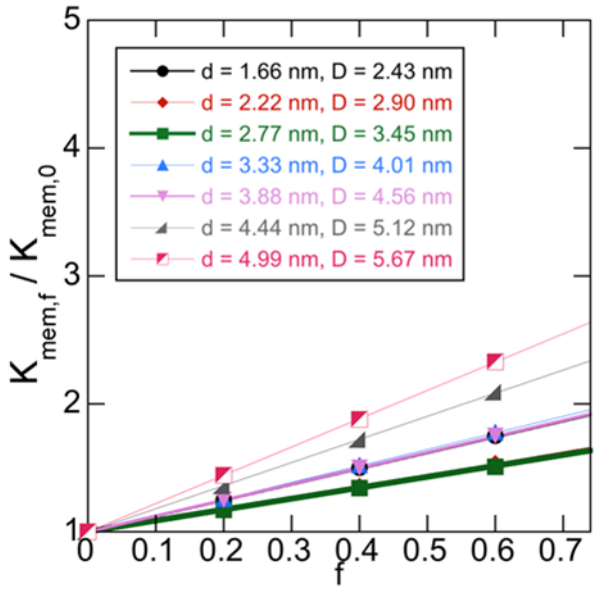

Figure 5. Water permeability increase *versus* surface area fraction occupied by DWNTs, *f*, for a DWNT chitosan membrane with different internal and external diameters.

3.2 Selectivity prediction

As discussed in the introduction, two small molecules, rac-fluoxetine and glucose, difficult to separate from water have been selected for the selectivity analysis, plus ethanol whose separation from water has industrial relevance. The permeability analysis, carried out in the previous section, showed that the MWNT with internal diameters of 4.44 nm provides the best compromise between permeability enhancement, density of vertically aligned nanotubes and the inlet CNT's width for an effective functionalization. As such, it was decided to functionalize the 4.44 nm tubes to try to maximize selectivity while retaining the higher permeability.

When steric hindrance is considered as the driving force for molecular rejection, this can be assumed to be proportional to $1-\Sigma$ where $\Sigma = A_{mol,perm} / A_{CNT,free}$. Molecular rejection for the target compounds is reported in Table 1 for each of the functionalization models tested (shown in Fig. 2). It is clear that the

choice of the 4.44 nm tubes to maximize permeability has somewhat detrimental effects on their selectivity to small molecules. Nonetheless, significant increases in rejection were obtained compared to the un-functionalized tubes, where essentially no rejection was observed.

Table 1. Molecular rejection $1-\Sigma$ for the four target compounds for a 4.44 nm tube with functionalized tips using different PIM-monomers (FGs).

Molecule	$1-\Sigma$ (%)					
	A-model FG				B-model FG	
	$2,1A^{IN}$	$2,1A^{OUT}$	$3,1A^{IN}$	$3,1A^{OUT}$	$2,2B^{IN\text{-}OUT}$	$3,2B^{IN\text{-}OUT}$
rac-Fluoxetine	60	41	86	52	82	91
Glucose	50	35	71	44	72	85
Ethanol	35	25	50	33	57	73
Water	23	18	34	25	42	55

In particular, an increase in rejection of a factor of 2.5 and 2 for rac-fluoxetine and glucose, respectively, compared to water was found when the A models were used. A smaller increase is found for ethanol-to-water rejection, for the same FGs steric hindrance, due to their more comparable MCS, as expected. When B models were used, the rejection enhancements were slightly reduced.

It is worth noting that the $1-\Sigma$ values also provide accurate information on the structure-property relationship, in this case functionalization model-rejection. Consequently, using the proposed computational approach, molecular rejection of target solutes, for a fixed MWNT internal diameter, can be controlled by the number of the PIM-1 monomers (constituting the FGs) and in turn by the number of FGs anchored on the CNT inlet. For example, Table 1 shows that a sharp rejection of the rac-fluoxitine, 86 % with a rejection increase by a factor of 2.5 compared to water molecules, is achieved using the $3,1A^{IN}$. This sharp rejection is primarily caused by the orientation of the FGs with respect to the CNTs entrance, and not simply by the increased number of FGs from 2 to 3 (cfr. $3,1A^{IN}$ and $3,1A^{OUT}$). This conclusion is also confirmed by observing the rejections obtained using 2 or 3 FGs B type regardless of their monomer number.

In the permeability and selectivity optimization of MWNTs membranes, a key point is to maximize the rejection of solutes while at the same time maximizing the solvent (water) permeation, i.e. minimize

the water entrance effect [47]. Therefore, although, 3,2$B^{IN\text{-}OUT}$ yields the highest rejection for rac-fluoxetine, the best rac-fluozetine-to-water rejection ratio is given instead by configuration 3,1A^{IN} because using this functionalized model rac-fluozetine-to-water $1-\Sigma$ ratio is bigger than the analogous ratio between the rejections obtained with the 3,2$B^{IN\text{-}OUT}$.

Similar conclusions can be drawn for glucose and ethanol, with smaller ratios obtained for the latter. Although commercial membranes with better solute-water rejection ratios than the ones reported here exist, the value of this work lies in the presentation of a novel design methodology to optimize both selectivity and permeability for CNT-polymer membranes without recourse to any fitting.

As anticipated at the end of section 2.3, several other FGs such as oligo-ethylene glycol and silanes groups were investigated. Both classes of analyzed chemical groups have aliphatic chains with different rotation angles. Due to several rotamers present in the aliphatic chains constituting the latter functional groups, a conformational analysis was required. The multiple degrees of freedom in oligo-ethylene glycol and silane groups imply that the winding of these functional groups does not provide a sufficient steric hindrance at the 4.44 nm diameter nanotube inlets. It is very important to emphasize that the assessment of the steric hindrance of all tested groups was made on the basis of $1-\Sigma$ values with respect to the un-functionalized tubes, using the more probable conformers carried out from the conformational analysis. Therefore, the novel proposed computational methodology can be used to estimate, through a comparative analysis but quantitative and rigorous, the steric effect of different functional groups to be used for decorating nanopores with rigid or well defined forms.

Conclusions

A novel computational method to optimize the selectivity-permeability of functionalized CNT-polymer membranes was presented in this study, with the aim of achieving a high rejection of organic solutes with low molecular weight without a marked fall in water permeability. MWNTs with specific internal and external diameters matching commercially available tubes were functionalized with PIM-1 monomer based groups. The methodology is of general use and requires no fitting parameter, only the chemical structure of the solute to test.

The permeability optimization showed that aligning the tubes can yield up to 3 orders of magnitude increase in flux compared to a virgin TFC membrane, whereas randomly aligned tubes only double the flux. The proposed computational method also revealed that in the selection of MWNTs, both the external and innermost tubes' diameters have to be considered to maximize permeability, since no

water can flow through the tube's interlayers. This point was even more evident for a high flux chitosan membrane where the use of thick MWNTs induced a decrease in permeability whereas the use of thin DWNTs generated a modest increase in permeability.

A novel algorithm, free from any fitting (adjustable) or empirical parameters, is proposed to evaluate the steric hindrance due to FGs anchored on the CNT inlet. Using a large 4.44 nm diameter MWNT it was nonetheless possible to achieve high rejection of small solutes by functionalizing the tip of the MWNTs using the PIM-1 monomers, as functional groups. In recent years, many other PIMs have been synthesized with components that are more rigid than PIM-1; thus, the method proposed in this work allows predicting the rejection capabilities of these novel PIMs functional groups. The combination of a large tube diameter and tip functionalization could yield higher flow and rejection for a MWNT-polymer membrane, assuming that a suitable method to align the tubes perpendicularly to the membrane surface can be found and used on a large scale.

Acknowledgments

The research leading to these results has received funding from the European Community's Seventh Framework Programme BioNexGen (Grant agreement no. CP-FP 246039-2) EU FP/ project. The authors are grateful to the CINECA for the use of High Performance Computers and Prof. Bartolo Gabriele (University of Calabria) for useful scientific discussion.

Reference

[1] G. Hummer, J.C. Rasaiah, J.P. Noworyta, Water Conduction through the Hydrophobic Channel of a Carbon Nanotube, Nature, 414 (2001) 188-190.
[2] A. Striolo, The Mechanism of Water Diffusion in Narrow Carbon Nanotubes, Nano Lett., 6 (2006) 633 -639.
[3] M. Whitby, N. Quirke, Fluid Flow in Carbon Nanotubes and Nanopipes, Nat. Nano., 2 (2007) 87-94.
[4] D. Mattia, K.P. Lee, F. Calabrò, Water permeation in carbon nanotube membranes, Current Opinion in Chemical Engineering, 4 (2014) 32-37.
[5] D. Mattia, H. Leese, K.P. Lee, Carbon nanotube membranes: From flow enhancement to permeability, J. Membr. Sci., 475 (2015) 266-272.
[6] M. Majumder, N. Chopra, R. Andrews, B.J. Hinds, Nanoscale hydrodynamics: Enhanced Flow in Carbon Nanotubes, Nature, 438 (2005) 44.
[7] S. Kim, F. Fornasiero, H.G. Park, J.B. In, E. Meshot, G. Giraldo, M. Stadermann, M. Fireman, J. Shan, C.P. Grigoropoulos, O. Bakajin, Fabrication of flexible, aligned carbon nanotube/polymer composite membranes by in-situ polymerization, J. Membr. Sci., 460 (2014) 91-98.
[8] Y. Baek, C. Kim, D.K. Seo, T. Kim, J.S. Lee, Y.H. Kim, K.H. Ahn, S.S. Bae, S.C. Lee, J. Lim, K. Lee, J. Yoon, High performance and antifouling vertically aligned carbon nanotube membrane for water purification, J. Membr. Sci., 460 (2014) 171-177.
[9] J.K. Holt, H.G. Park, Y. Wang, M. Stadermann, A.B. Artyukhin, C.P. Grigoropoulos, A. Noy, O. Bakajin, Fast Mass Transport Through Sub-2-Nanometer Carbon Nanotubes, Science, 312 (2006) 1034-1037.

[10] M. Majumder, N. Chopra, B.J. Hinds, Mass Transport through Carbon Nanotube Membranes in Three Different Regimes: Ionic Diffusion and Gas and Liquid Flow, ACS Nano, 5 (2011) 3867-3877.
[11] B. Corry, Water and ion transport through functionalised carbon nanotubes: implications for desalination technology, Energy & Environmental Science, 4 (2011) 751-759.
[12] M. Whitby, L. Cagnon, M. Thanou, N. Quirke, Enhanced Fluid Flow through Nanoscale Carbon Pipes, Nano Lett., 8 (2008) 2632-2637.
[13] K.P. Lee, T.C. Arnot, D. Mattia, A review of reverse osmosis membrane materials for desalination--Development to date and future potential, J. Membr. Sci., 370 (2011) 1-22.
[14] W.-F. Chan, H.-y. Chen, A. Surapathi, M.G. Taylor, X. Shao, E. Marand, J.K. Johnson, Zwitterion Functionalized Carbon Nanotube/Polyamide Nanocomposite Membranes for Water Desalination, ACS Nano, 7 (2013) 5308-5319.
[15] H.A. Shawky, S.-R. Chae, S. Lin, M.R. Wiesner, Synthesis and characterization of a carbon nanotube/polymer nanocomposite membrane for water treatment, Desalination, 272 (2011) 46-50.
[16] C. Tang, Q. Zhang, K. Wang, Q. Fu, C. Zhang, Water transport behavior of chitosan porous membranes containing multi-walled carbon nanotubes (MWNTs), J. Membr. Sci., 337 (2009) 240-247.
[17] H. Wu, B. Tang, P. Wu, Optimization, characterization and nanofiltration properties test of MWNTs/polyester thin film nanocomposite membrane, J. Membr. Sci., 428 (2013) 425-433.
[18] J.-H. Choi, J. Jegal, W.-N. Kim, Fabrication and characterization of multi-walled carbon nanotubes/polymer blend membranes, J. Membr. Sci., 284 (2006) 406-415.
[19] G. De Luca, E. Tocci, E. Drioli, Quantum and molecular mechanics calculations on modified silica nano ring, J. Mol. Struct., 739 (2005) 163-172.
[20] M. Majumder, N. Chopra, B.J. Hinds, Effect of Tip Functionalization on Transport through Vertically Oriented Carbon Nanotube Membranes, J. Am. Chem. Soc., 127 (2005) 9062-9070.
[21] D. Mattia, Y. Gogotsi, Review: static and dynamic behavior of liquids inside carbon nanotubes, Microfluid. Nanofluid., 5 (2008) 289-305.
[22] W.D. Nicholls, M.K. Borg, D.A. Lockerby, J.M. Reese, Water transport through carbon nanotubes with defects, Mol. Simul., 38 (2012) 781-785.
[23] K. Ritos, D. Mattia, F. Calabrò, J.M. Reese, Flow enhancement in nanotubes of different materials and lengths, J. Chem. Phys., 140 (2014).
[24] W. Nicholls, M. Borg, D. Lockerby, J. Reese, Water transport through (7,7) carbon nanotubes of different lengths using molecular dynamics, Microfluid. Nanofluid., 12 (2012) 257-264.
[25] D. Mattia, F. Calabrò, Explaining high flow rate of water in carbon nanotubes via solid–liquid molecular interactions, Microfluid. Nanofluid., 13 (2012) 125-130.
[26] F. Calabrò, K.P. Lee, D. Mattia, Modelling flow enhancement in nanochannels: Viscosity and slippage, Applied Mathematics Letters, 26 (2013) 991-994.
[27] D.-Y. Kang, C.W. Jones, S. Nair, Modeling molecular transport in composite membranes with tubular fillers, J. Membr. Sci., 381 (2011) 50-63.
[28] P.J.F. Harris, Carbon Nanotubes and Related Structures, Cambridge University Press, Cambridge, UK, 1999.
[29] J.A. Thomas, A.J.H. McGaughey, Reassessing Fast Water Transport Through Carbon Nanotubes, Nano Lett., 8 (2008) 2788-2793.
[30] S.-I. Nakao, S. Kimura, Models of Membrane Transport Phenomena and their Applications for Ultrafiltration Data, J. Chem. Eng. Jpn., 15 (1982) 200-205.
[31] B. Van Der Bruggen, J. Schaep, D. Wilms, C. Vandecasteele, A Comparison of Models to Describe the Maximal Retention of Organic Molecules in Nanofiltration, Sep. Sci. Technol., 35 (2000) 169-182.
[32] F. Bisignano, Modeling of nanostructured membranes for wastewater purification, in: Dottorato in Scienza e Tecnica Bernardino Telesio Curriculum M3, XXVI ciclo, Università della Calabria, Italy, 2014.
[33] A. Buekenhoudt, F. Bisignano, G. De Luca, P. Vandezande, M. Wouters, K. Verhulst, Unravelling the solvent flux behaviour of ceramic nanofiltration and ultrafiltration membranes, J. Membr. Sci., 439 (2013) 36-47.

[34] G. De Luca, F. Bisignano, V.G. Mavrantzas, E. Karahaliou, G. Voyiatzis, J. Hoinkis, A. Figoli, Rejection of Low Molecular Weight Solutes by Mean of Cnts: A Quantum Mechanics and Atomistic Study, Procedia Engineering, 44 (2012) 371-372.
[35] N.B. McKeown, P.M. Budd, Polymers of intrinsic microporosity (PIMs): organic materials for membrane separations, heterogeneous catalysis and hydrogen storage, Chem. Soc. Rev., 35 (2006) 675-683.
[36] T.P. Straatsma, E. Apra, T.L. Windus, M.E. Dupuis, J. Bylaska, W. de Jong, NWChem, A computational chemistry package for parallel computers, version 6.1.1, in, Pacific Northwest National Laboratory, 2011.
[37] X. Xu, Q. Zhang, R.P. Muller, W.A. Goddard, An extended hybrid density functional (X3LYP) with improved descriptions of nonbond interactions and thermodynamic properties of molecular systems, The Journal of Chemical Physics, 122 (2005) -.
[38] K.B. Jirage, J.C. Hulteen, C.R. Martin, Nanotubule-Based Molecular-Filtration Membranes, Science, 278 (1997) 655-658.
[39] S.B. Lee, D.T. Mitchell, L. Trofin, T.K. Nevanen, H. Söderlund, C.R. Martin, Antibody-Based Bio-Nanotube Membranes for Enantiomeric Drug Separations, Science, 296 (2002) 2198-2200.
[40] T.-S. Chung, L.Y. Jiang, Y. Li, S. Kulprathipanja, Mixed matrix membranes (MMMs) comprising organic polymers with dispersed inorganic fillers for gas separation, Progress in Polymer Science, 32 (2007) 483-507.
[41] S. Dapprich, I. Komáromi, K.S. Byun, K. Morokuma, M.J. Frisch, A new ONIOM implementation in Gaussian98. Part I. The calculation of energies, gradients, vibrational frequencies and electric field derivatives, Journal of Molecular Structure: THEOCHEM, 461–462 (1999) 1-21.
[42] K. Kitaura, K. Morokuma, A new energy decomposition scheme for molecular interactions within the Hartree-Fock approximation, Int. J. Quantum Chem., 10 (1976) 325-340.
[43] J.C. Slater, K.H. Johnson, Self-Consistent-Field Xα Cluster Method for Polyatomic Molecules and Solids, Phys. Rev. B, 5 (1972) 844-853.
[44] T. Yamada, T. Namai, K. Hata, D.N. Futaba, K. Mizuno, M. Yudasaka, M. Yumura, S. Iijima, Size-selective growth of double-walled carbon nanotube forests from engineered iron catalysts, Nat. Nano., 1 (2006) 131-136.
[45] L. Braeken, R. Ramaekers, Y. Zhang, G. Maes, B.V.d. Bruggen, C. Vandecasteele, Influence of hydrophobicity on retention in nanofiltration of aqueous solutions containing organic compounds, J. Membr. Sci., 252 (2005) 195-203.
[46] J.L.C. Santos, P. de Beukelaar, I.F.J. Vankelecom, S. Velizarov, J.G. Crespo, Effect of solute geometry and orientation on the rejection of uncharged compounds by nanofiltration, Separation and Purification Technology, 50 (2006) 122-131.
[47] D. Cohen-Tanugi, J.C. Grossman, Water Desalination across Nanoporous Graphene, Nano Lett., 12 (2012) 3602-3608.